Fast Variance Prediction for Iterative Reconstruction of 3D Helical CT Images

Stephen M. Schmitt and Jeffrey A. Fessler

***Abstract*—Fast variance prediction for iteratively-reconstructed helical CT images is useful for analysis of resulting images and potentially for dynamic dose adjustment during a scan. Previous methods require impractical computation times to approximate the image variance; other methods are able to approximate variance quickly but only for specific CT geometries, excluding 3D helical CT. In this paper we present an extension of these previous fast methods to predict the variance of iteratively reconstructed images for third-generation 3D helical CT scans. We compare this method in computation time and error to the empirical variance derived from multiple simulated reconstruction realizations.**

I. Introduction

Iterative reconstruction (IR) methods for computed tomography are receiving increased attention for their improved resolution and noise properties compared to FBP [7]. However, the statistical properties of IR reconstructions are difficult to compute compared to FBP. Closed-form but computationally intractable expressions exist [1] for the mean and covariance matrix of the reconstruction when the weighting matrix $\mathbf{W}$ and covariance of the projections are given, so faster prediction methods are desirable.

Prior work has exploited approximate local shift-invariance to develop FFT-based approximations for the variance map of the image, i.e., the diagonal of the covariance matrix, for arbitrary system geometries [5]. Unlike empirical methods, which can only be used to find the variance map of the entire image simultaneously, these FFT-based methods can approximate the variance of one specific voxel of interest at a time. However, these FFT-based methods are computationally intensive; they are useful for theoretical analysis but require projection and back-projection of each voxel of interest and are unsuitable for producing a variance map for a whole volume. There are methods for 2D fan-beam [9], 3D step-and-shoot [10], and 3D axial CT [6] that make further approximations to greatly reduce the computational load of this method and make it suitable for predicting variance maps for an entire volume. None of these methods, though, apply directly to 3D helical CT.

In this paper, we adapt [6] to the problem of predicting approximate variance maps for iterative reconstruction of 3D helical CT scans. Like this prior work, the computational cost of the variance approximation is reduced by several orders of magnitude compared to empirical estimation or the FFT-based method in [5] for CT.

This work was supported in part by NIH grant R01 HL-098686 and by equipment donations from Intel.

Stephen M. Schmitt and Jeffrey A. Fessler are with the Department of Electrical Engineering and Computer Science, University of Michigan, Ann Arbor, MI 48109 USA (smschm@umich.edu, fessler@umich.edu)

II. Methods

A reconstruction method using a weighted least squares data-fit term using log-sinogram observations $\mathbf{y}$, system matrix $\mathbf{A}$ and a regularization term R is given by

$$\hat{\mathbf{x}} = \operatorname{argmin}_{\mathbf{x}} \frac{1}{2}||\mathbf{y}-\mathbf{A}\mathbf{x}||^2_{\mathbf{W}} + \frac{\alpha}{2} R(\mathbf{x}). \tag{1}$$

With a weighting matrix $\mathbf{W} = \operatorname{cov}(\mathbf{y})^{-1}$ and assuming that the minimization algorithm is iterated until convergence, the covariance matrix of $\hat{\mathbf{x}}$ in (1) is approximately [1]:

$$\operatorname{cov}(\hat{\mathbf{x}}) \approx (\mathbf{H}+\alpha\nabla^2 R(\hat{\mathbf{x}}))^{-1}\mathbf{H}(\mathbf{H}+\alpha\nabla^2 R(\hat{\mathbf{x}}))^{-1}. \tag{2}$$

If $R(\mathbf{x}) = \sum_i \psi([\mathbf{C}\mathbf{x}]_i)$ for a matrix $\mathbf{C}$ and a convex penalty function ψ that is twice-differentiable in an open set containing 0 with $\psi(0) = \psi'(0) = 0$, $\psi''(0) = 1$, then

$$\nabla^2 R(\mathbf{x}) = \mathbf{C}^{\mathrm{T}}\ddot{\Psi}(\mathbf{x})\mathbf{C}, \tag{3}$$

where $\ddot{\Psi}(\mathbf{x})$ is a diagonal matrix with $[\ddot{\Psi}(\mathbf{x})]_{jj} = \psi''([\mathbf{C}\mathbf{x}]_j)$. With a sufficiently large α, we would expect that, for most voxels, $[\mathbf{C}\mathbf{x}]_j$ is small and in the twice-differentiable region of ψ and therefore, that $\ddot{\Psi}(\hat{\mathbf{x}}) \approx \mathbf{I}$ is a valid approximation except near edges between regions of different attenuation coefficients in the image. Making this substitution transforms (2) into

$$\operatorname{cov}(\hat{\mathbf{x}}) \approx (\mathbf{H}+\alpha\mathbf{C}^{\mathrm{T}}\mathbf{C})^{-1}\mathbf{H}(\mathbf{H}+\alpha\mathbf{C}^{\mathrm{T}}\mathbf{C})^{-1}, \tag{4}$$

where $\mathbf{H} \triangleq \mathbf{A}^{\mathrm{T}}\mathbf{W}\mathbf{A}$. However, direct computation of this matrix is not computationally tractable.

A. Prior work

In [6], we define a continuous-frequency response operator *local* to the jth voxel:

$$\left(\mathscr{F}^3_{j,\text{cont}}\{\mathbf{x}\}\right)(\vec{\nu}) = \sum_{\ell=1}^{|\vec{N}|} \mathbf{x}_\ell \exp\left(-\imath 2\pi\vec{\nu}\cdot(\vec{n}_\ell - \vec{n}_j)\right), \tag{5}$$

where $\vec{n}_j$ is the position, in 3 integer coordinates, of the voxel j. We show that the variance of this voxel j can be estimated by:

$$\operatorname{var}(\hat{\mathbf{x}}_j) \approx \int_{[-\frac{1}{2},\frac{1}{2}]^3} \frac{H_j(\vec{\nu})}{(H_j(\vec{\nu})+\alpha R(\vec{\nu}))^2} \mathrm{d}\vec{\nu}, \tag{6}$$

where $H_j \triangleq \mathscr{F}^3_{j,\text{cont}}\{\mathbf{H}_{*j}\}$, representing the frequency response of projection, weighting, and back-projection, and $R \triangleq \mathscr{F}^3_{j,\text{cont}}\{[\mathbf{C}^{\mathrm{T}}\mathbf{C}]_{*j}\}$, representing the frequency response of the regularizer when $[\mathbf{Cx}]_j \approx 0$.

We also show that $H_j(\vec{\nu})$ can be written as $H_j(\vec{\nu}) \approx K \cdot J(\vec{\nu}) \cdot E_j(\Phi)$. Here, J depends only on the spatial frequency and not the image or voxel location. E_j is dependent on the image and voxel location but only depends on the spatial frequency via its angle Φ in cylindrical coordinates (ρ, Φ, ν_3). When H_j is specified in this form, (6) can be rewritten in a single-integral form:

$$\operatorname{var}(\hat{\mathbf{x}}_j) \approx \alpha^{-1} \int_0^{2\pi} F(\Phi, \alpha^{-1} K E_j(\Phi))\, \mathrm{d}\Phi, \tag{7}$$

where

$$F(\Phi,\gamma) \triangleq \int_0^{\rho_{\max}(\Phi)} \int_{-\frac{1}{2}}^{\frac{1}{2}} \frac{\gamma \cdot J(\rho,\Phi,\nu_3)\cdot \rho}{(\gamma \cdot J(\rho,\Phi,\nu_3) + R(\vec{\nu}))^2}\, \mathrm{d}\nu_3\, \mathrm{d}\rho. \tag{8}$$

There is no closed form for (8), but we can numerically integrate and tabulate it for many values of Φ and γ, independently of the image or weighting matrix, for a given CT geometry and regularizer. In doing so, variance estimation via (7) is simply a one-dimensional numerical integration of values looked up in a pre-computed table of F.

We can import much of the derivation in [6] to apply to helical CT instead of axial CT. In particular, we can still approximate $H_j(\vec{\nu}) \approx K \cdot J(\vec{\nu}) \cdot E_j(\Phi)$, where for helical CT one can show:

$$K = \Delta_x^3 \Delta_z D_{sd}^2 / D_{s0}^2 \Delta_s \Delta_t \Delta_\beta \tag{9}$$

$$J(\rho,\Phi,\nu_3) = \frac{\operatorname{sinc}(\rho\cos\Phi)^2 \operatorname{sinc}(\rho\sin\Phi)^2 \operatorname{sinc}(\nu_3)^2}{\rho} \tag{10}$$

$$E_j(\Phi) = \sum_{\beta\in\mathscr{B}_j(\Phi)} \frac{D_{s0}^2 \mathring{w}_{\beta,j}}{D_{\beta,j}\sqrt{D_{s0} - r_j^2 \cos^2(\phi_j - \Phi)}}. \tag{11}$$

Here, Δ_x is the spacing between voxels in the x and y directions; Δ_z is the spacing between voxels in the z direction; Δ_s, Δ_t are the spacings between pixels on the detector in the s and t directions; Δ_β is the spacing (in radians) of detector angles between views; D_{sd} is the distance from the x-ray source to the detector; D_{s0} is the distance from the source to the isocenter; $D_{\beta,j}$ is the distance from the source to the voxel j when the source is at angle β; r_j is the distance from the isocenter to voxel j; ϕ_j is the angle of voxel j when represented in cylindrical coordinates. All distances given above ignore the z-coordinate; all points are projected into the xy-plane before calculating distances. The only term dependent on the object is $\mathring{w}_{\beta,j}$, which is discussed further in the next section.

B. Modification for helical CT

The items changed by the transition to helical CT are $\mathscr{B}_j(\Phi)$, which is the set of source angles β that solve

$$r_j \cos(\phi_j - \Phi) = D_{s0}\cos(\beta - \Phi), \tag{12}$$

and $\mathring{w}_{\beta,j}$. The term $\mathring{w}_{\beta,j}$ is the element of the statistical weighting matrix $\mathbf{W}$ corresponding to the location on the detector where a ray from the source at angle β passing through the voxel j lands (or 0, if this ray does not land on the detector).

Equation (12) is not changed by the transition to helical CT, but the values of β that solve it are different. The solutions are the set of source angles for which the ray passing through voxel j is perpendicular to the frequency vector $\vec{\nu}$, where the ray and frequency vector are *both* projected into the xy-plane.

For axial CT, the set $\mathscr{B}_j$ is given by:

$$\mathscr{B}_j(\Phi) = \{\beta^+, \beta^-\} = \left\{\Phi \pm \arccos\left(\frac{r_j}{D_{s0}}\cos(\phi_j - \Phi)\right)\right\}. \tag{13}$$

This covers all of the solutions in one turn, which covers a maximum range of 2π. For helical CT with an arbitrary starting and ending angles $\beta_{\min}$, $\beta_{\max}$,

$$\mathscr{B}_j(\Phi) = \left\{\Phi \pm \arccos\left(\frac{r_j}{D_{s0}}\cos(\phi_j - \Phi)\right) + k2\pi\right\} \cap [\beta_{\min}, \beta_{\max}] \tag{14}$$

for $k \in \mathbb{Z}$. Axial CT is then a special case of (14). Since a large part of the computational cost of our method is finding (11), the change to helical CT increases the cost of our algorithm linearly in the number of turns.

The other quantity, $\mathring{w}_{\beta,j}$, is unchanged except that the lookup procedure is computed for helical CT instead of axial CT.

III. Results

To evaluate our prediction for the variance map, we compared it to the variance map derived empirically by simulating 93 reconstructions of a $512 \times 512 \times 500$ XCAT phantom (Fig. 1 displays axial, sagittal, and coronal slices) with voxel size $\Delta_x, \Delta_y = 0.977\text{mm}, \Delta_z = 0.625\text{mm}$. The system geometry, based on a third-generation GE helical CT scanner, had $\Delta_s \times \Delta_t = 1.0239 \times 1.0964\text{mm}$ detector element size, $D_{sd} = 949.075\text{mm}$ source-to-detector distance, and $D_{s0} = 408.075\text{mm}$ source-to-isocenter distance. In our simulations, the X-ray source went through 3 rotations of 984 views each, with a pitch of 1. Each reconstruction used an ordered-subset method with 41 subsets for 100 iterations.

The regularization used a first-order differencing matrix $\mathbf{C}$ that considered the 6 face-neighbors of each voxel. These differences were penalized by a Huber cost function:

$$\psi(x) = \begin{cases} x^2/2, & |x| \le \delta \\ \delta|x| - \delta^2/2, & |x| > \delta \end{cases},$$

which satisfies our criteria for cost functions. The value of δ was 200HU. The regularization parameter α was equal to 128. The weighting $\mathbf{W}$ was normalized so that unattenuated rays had a weight of 1. The simulated X-ray beam intensity was 10^5 photons per view. For simplicity, we used a standard edge-preserving regularizer, rather than the modified regularizer considered in [2].

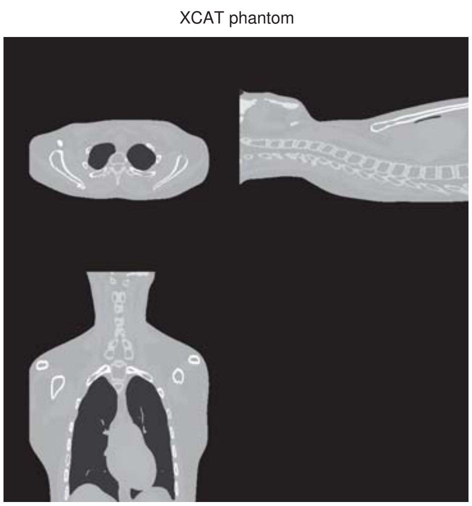

Fig. 1. XCAT phantom (top left is transaxial slice through center of volume; bottom left is center coronal slice; top right is center sagittal slice.)

Figure 2 shows axial, sagittal, and coronal slices of the image of the empirical standard deviation from our simulated reconstructions. Since the results were noisy and the ground truth standard deviation is slowly varying, we blurred the empirical image with a gaussian kernel with a FWHM of 4 voxels each in the x and y directions. Figure 3 shows the corresponding image from our approximation. Since standard deviation varies slowly, we only compute it once per $4 \times 4 \times 4$ block and use nearest-neighbor interpolation to fill in the rest. More sophisticated interpolation could be used, but the interpolation error is minimal compared to the intrinsic error of our method. Figure 4 shows the magnitude of the error of our approximated standard deviation. Figure 5 shows both the empirical and approximated standard deviation along a one-dimensional profile through a z-axis of the image. The spike in the empirical map near the end of the axial FOV is due to a suboptimal OS algorithm implementation that is somewhat unstable in regions where the helical sampling is poor. The OS algorithm in [4] would reduce this instability and reduce the empirical variance in the end slices.

The computation time of our method for the entire volume using $4 \times 4 \times 4$ downsampling was 1040 CPU-seconds using one core of an Intel Core i7-860 with 16 GB of memory. The empirical reconstructions took a total of 300.8 CPU-days each using one core of an Intel X5650 processor also with 16GB of memory; the range for the individual reconstructions was 2.58 to 3.89 CPU-days.

The axial modulations seen in the coronal and sagittal noise maps were a new phenomena in helical CT variance maps that we had not observed in our previous 3D axial

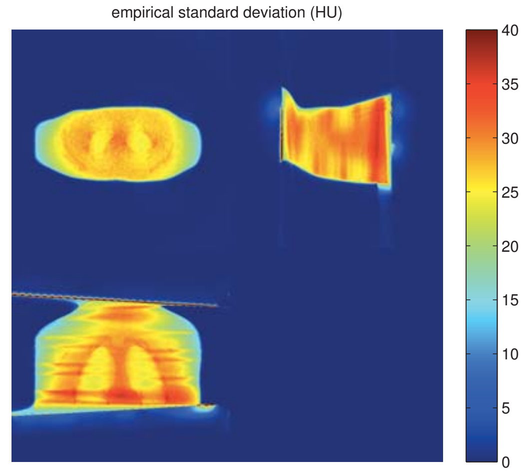

Fig. 2. Empirical standard deviation

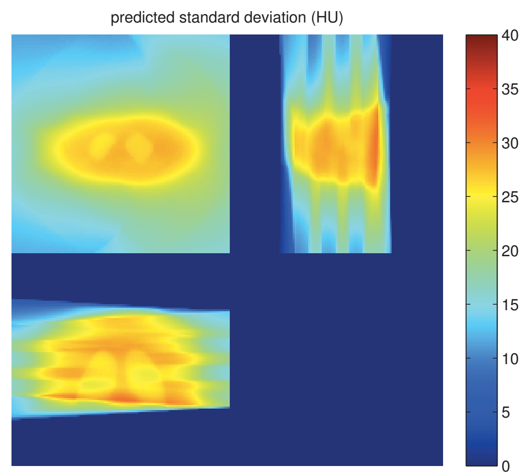

Fig. 3. Predicted standard deviation

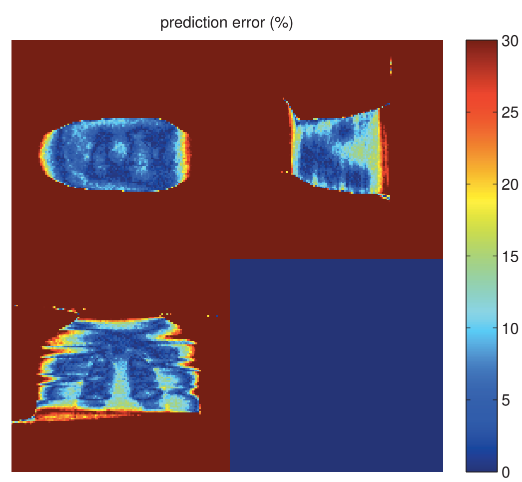

Fig. 4. Error in predicted standard deviation

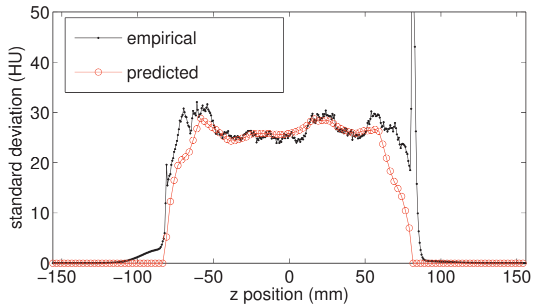

Fig. 5. Empirical & Predicted z-slice through object

CT noise predictions [6]. To help explain this behaviour, we computed a 3D map that shows for each voxel how many rays intersect that voxel. Intuitively, voxels with more intersecting rays are better sampled and thus may have lower variance. Figure 6 shows slices through this ray counting map, and indeed we observe that the sampling pattern influences the predicted and empirical noise maps.

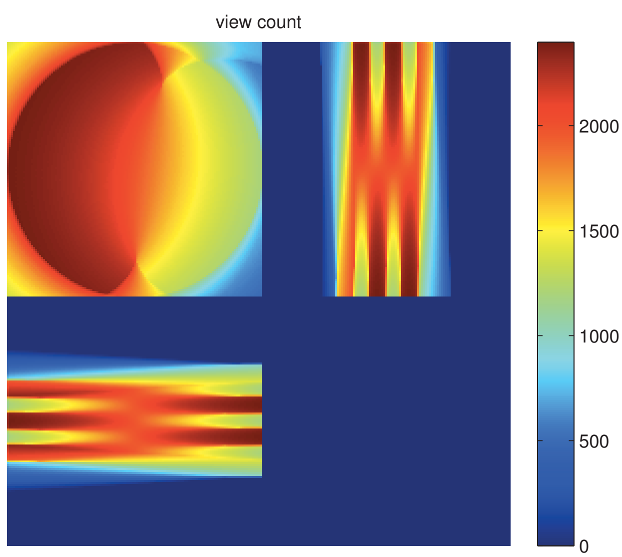

Fig. 6. Count of views that contribute to each voxel's variance prediction

IV. Discussion

The presented methods are able to predict the standard deviation of most voxels in the reconstructed image within an error of 20% in less time than the amount of time empirical measurement takes by a factor of over 10000. The more general (and accurate) approximation using a forward- and back-projection takes 2400 CPU-seconds per voxel (using the same Intel Core i7 above), a factor of over $4 \cdot 10^6$ times as long as our method for one voxel. Whether the tradeoff for time at the expense of accuracy provided by our method is acceptable depends on the application. We also note that our methods would be applicable to axial CT, including short scans, as a special case.

Outside the support of the object there is significant approximation error because our method ignores the non-negativity constraint of the reconstruction. The empirical variance outside the object approaches zero, and so the relative error of our method (which does not go to zero) becomes infinite. An extension to our method could use a pilot reconstruction or masking method (e.g. [3]) to identify external air regions and simply estimate the variance as zero, or use a separate approximation that is more suitable for these regions.

V. Conclusions

In this paper, we have presented a method that is able to approximate the variance of each voxel of a 3D helical CT image reconstructed using a penalized weighted least-squares formulation. This method has a computational cost that is smaller by several orders of magnitude compared to existing variance prediction methods for helical CT, while maintaining a reasonable error within regions of interest.

One direction of future work will be investigating the effect of mismatch between the weighting matrix used for reconstruction and the "optimal" weighting matrix, the inverse of the sinogram covariance. Since the covariance matrix of the sinogram is unknown, in practice we can only approximate it. Knowing the effect of mismatch would also be useful for cases where mismatch is intentional, e.g. [8], to mask out observations known to cause artifacts.

References

[1] J. A. Fessler. Mean and variance of implicitly defined biased estimators (such as penalized maximum likelihood): Applications to tomography. *IEEE Trans. Im. Proc.*, 5(3):493–506, March 1996.

[2] J. A. Fessler and W. L. Rogers. Spatial resolution properties of penalized-likelihood image reconstruction methods: Space-invariant tomographs. *IEEE Trans. Im. Proc.*, 5(9):1346–58, September 1996.

[3] J. Gregor. Data-driven problem reduction for image reconstruction from projections using gift wrapping. *Nuclear Science, IEEE Transactions on*, 58(3):724–729, 2011.

[4] D. Kim, D. Pal, J-B. Thibault, and J. A. Fessler. Improved ordered subsets algorithm for 3D X-ray CT image reconstruction. In *Proc. 2nd Intl. Mtg. on image formation in X-ray CT*, pages 378–81, 2012.

[5] J. Qi and R. M. Leahy. A theoretical study of the contrast recovery and variance of MAP reconstructions from PET data. *IEEE Trans. Med. Imag.*, 18(4):293–305, April 1999.

[6] S. Schmitt and J. A. Fessler. Fast variance computation for quadratically penalized iterative reconstruction of 3D axial CT images. In *Proc. IEEE Nuc. Sci. Symp. Med. Im. Conf.*, pages 3287–92, 2012.

[7] J-B. Thibault, K. Sauer, C. Bouman, and J. Hsieh. A three-dimensional statistical approach to improved image quality for multi-slice helical CT. *Med. Phys.*, 34(11):4526–44, November 2007.

[8] K. Zeng, B. De Man, and J-B. Thibault. Correction of iterative reconstruction artifacts in helical cone-beam CT. In *Proc. Intl. Mtg. on Fully 3D Image Recon. in Rad. and Nuc. Med*, pages 242–5, 2009.

[9] Y. Zhang-O'Connor and J. A. Fessler. Fast predictions of variance images for fan-beam transmission tomography with quadratic regularization. *IEEE Trans. Med. Imag.*, 26(3):335–46, March 2007.

[10] Y. Zhang-O'Connor and J. A. Fessler. Fast variance predictions for 3D cone-beam CT with quadratic regularization. In *Proc. SPIE 6510, Medical Imaging 2007: Phys. Med. Im.*, pages 65105W:1–10, 2007.